Carbohydrate Polymers 373 (2026) 124612

Contents lists available at ScienceDirect

Carbohydrate Polymers

journal homepage: www.elsevier.com/locate/carbpol

Solution conformational analysis of hyaluronan with different chain lengths by NMR spectroscopy

Yan Xue, Corine Sandström, Gustav Nestor *

Department of Molecular Sciences, Uppsala BioCenter, Swedish University of Agricultural Sciences, P.O. Box 7015, SE-750 07, Uppsala, Sweden

ARTICLE INFO

Keywords:
Hyaluronan
NMR spectroscopy
Conformational analysis
Glycosidic linkages

ABSTRACT

The solution conformation of hyaluronan (HA), a biopolymer in the glycosaminoglycan (GAG) family, is still not well understood despite its simple primary structure. The main origin of the structural flexibility of HA is its two alternating β(1 → 4) and β(1 → 3) glycosidic linkages and several studies have reported apparently contrasting evidence on the structural and dynamic behavior of these two linkages. Meanwhile, only short HA oligosaccharides have been investigated thoroughly by NMR spectroscopy and few studies have focused on comparisons between short and longer HA chains. We report herein a detailed conformational investigation of HA octasaccharide and 20-mer by NMR spectroscopy based on NOEs and ^{3}J-couplings, focusing on the glycosidic linkages and the *N*-acetyl group. This is the first NMR study that provides experimental support for the existence of minor conformations of the β(1 → 4) glycosidic linkage and validation of the predominant conformation of the β(1 → 3) glycosidic linkage previously established by MD simulations. This approach provides methodologies for conformational analysis among different chain lengths in other glycans.

1. Introduction

Hyaluronan (also known as hyaluronic acid, HA) is a linear glycosaminoglycan (GAG) of repeating disaccharide units consisting of D-glucuronic acid (GlcA) and *N*-acetyl-D-glucosamine (GlcNAc), which are linked by alternating $\beta(1 \rightarrow 4)$ and $\beta(1 \rightarrow 3)$ glycosidic linkages (Fig. 1). HA is present in all vertebrates and it is an essential constituent of the extracellular matrix (ECM). The most abundant amount of HA resides in skin tissue and the rest can be found in other connective tissues such as synovial fluid, the vitreous body, and the umbilical cord (Fraser et al., 1997). HA has a strong water-binding capacity due to its entangled chain structure with a polar hydrophilic face at physiological conditions, therefore HA is responsible for tissue hydration, lubrication, and space-filling (Fakhari & Berkland, 2013; van Dam et al., 2020). Despite the diversity of occurrence and functions of HA, it is a unique GAG since the simple primary structure has been preserved among all living organisms. Especially given the non-sulfated nature of HA, its variability of the primary structure lies only in the molecular size and polydispersity (Laurent & Fraser, 1992).

The higher-order structures of HA are more complex than its primary structure and have been investigated by many techniques over the years. Early structural studies of HA described that the molecule behaves as a random coil with an intrinsic stiffness (Laurent, 1955; Laurent et al., 1960). However, further investigations provided evidence that HA has a secondary structure involving both intra- and/or inter-molecular hydrogen bonds, which means the coiling of HA was not necessarily random (Almond, 2007; Giubertoni, Koenderink, & Bakker, 2019; Scott & Heatley, 1999). Additional studies have shown that components such as water molecules and cations also play key roles in defining HA conformation (Giubertoni et al., 2021; Guss et al., 1975; Heatley & Scott, 1988; Sheehan & Atkins, 1983). The first X-ray diffraction data indicated a helical structure of sodium hyaluronan fibers, but further crystallographic studies showed that there is a complex inter-conversion between double- and single-helices depending on the experimental conditions (Hargittai & Hargittai, 2008).

However, as to the locally dynamic structure of HA in solution, X-ray studies cannot fully reveal the organization of the chains. Almond et al. published a detailed structural analysis of HA by NMR spectroscopy and molecular dynamics (MD) simulations on three oligosaccharides (HA_4, HA_6, and HA_8), which proposed a contracted left-handed 4-fold helix model for the solution conformation of HA (Protein Data Bank accession code: 2BVK) (Almond et al., 2006). Furthermore, they also compared oligomer properties with polymeric HA and suggested that there is no discernible difference in amide proton environment between the

* Corresponding author.
E-mail address: gustav.nestor@slu.se (G. Nestor).

https://doi.org/10.1016/j.carbpol.2025.124612
Received 25 August 2025; Received in revised form 17 October 2025; Accepted 27 October 2025
Available online 28 October 2025

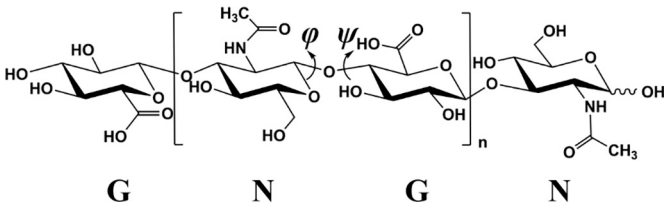

Fig. 1. Schematic structure of HA oligomers: HA_8 ($n = 3$) and HA_{20} ($n = 9$). Two torsion angles are shown over the $\beta(1 \rightarrow 4)$ glycosidic linkage between GlcA and GlcNAc: φ (H_1-C_1-O_4-C_4) and ψ (C_1-O_4-C_4-H_4). Similarly, the two torsion angles over the $\beta(1 \rightarrow 3)$ glycosidic linkage are defined as φ (H_1-C_1-O_3-C_3) and ψ (C_1-O_3-C_3-H_3).

polymer and the oligomer, which indicates that the HA octasaccharide can be representative of the conformation of the HA polymer (Blundell, DeAngelis, & Almond, 2006). Noticeably, only the interior part of the HA octasaccharide has been applied to mimic the HA polymer conformation due to end effects caused by the higher flexibility of the terminal residues of shorter chains (Blundell, DeAngelis, & Almond, 2006; Blundell, Reed, & Almond, 2006; Cowman et al., 1996; Cowman et al., 2001). However, other studies have shown that HA oligosaccharides and polysaccharides behave differently in terms of hydrogen-bonding network, self-association, and recognition by HA-binding proteins (Cowman, 2017). Their hydrodynamic properties can vary from nearly rod-like to weakly coiled, effectively spherical forms, and more apparent conformational variability has also been calculated for longer HA chains (Cowman, 2017; Taweechat et al., 2020).

The main origin of structural flexibility of both oligo- and polysaccharides of HA is the two β glycosidic linkages that are defined by the torsion angles φ and ψ (Fig. 1). Several contrasting pieces of evidence have been reported on structural and dynamic behavior around the β glycosidic linkages of HA (Cowman et al., 1996; Donati et al., 2001; Holmbeck et al., 1994). The MD prediction by Almond et al. indicated that both types of glycosidic linkages are restricted to a small region around $(\varphi, \psi) = (50°, 10°)$ with similar fluctuation around the global minimum (Almond et al., 2006). However, a more recent MD simulation study suggested that the $\beta(1 \rightarrow 4)$ linkage is more flexible than the $\beta(1 \rightarrow 3)$ linkage (Taweechat et al., 2020). In addition to the global minimum conformation, a number of MD simulations have shown a small percentage of *anti* conformation, thus a $\sim 180°$ difference in one of the torsion angles, placing the hydrogen atoms at the glycosidic linkage in *anti* conformation rather than the normal *syn* conformation (Fig. 2a and b) (Kutálková et al., 2020; Taweechat et al., 2020; Whitmore et al., 2020). Such minor conformations are more frequently observed over the $\beta(1 \rightarrow 4)$ linkage with a difference in the ψ torsion angle and have been referred to as flips that are responsible for turns in the HA structure (Kutálková et al., 2020). Previous NMR experiments on HA oligosaccharides (HA_8 and smaller) observed a chemical exchange between hydroxyl protons over the $\beta(1 \rightarrow 3)$ glycosidic linkage, which could be due to a minor *anti* conformation (Nestor et al., 2010), but no experimental evidence has been presented for such conformations in HA. Both the dynamics of the glycosidic linkages and the atypical minor *anti* conformation at the glycosidic linkages need to be further investigated experimentally in order to prove or disprove the very detailed predictions made by MD simulations.

Another source of conformational variability of HA is along the *N*-acetyl side group of GlcNAc. The amide proton of HA oligosaccharides is known to be in an *anti* orientation towards H2 (Fig. 2c) (Blundell, DeAngelis, & Almond, 2006). Several studies have investigated whether there is an inter-residue hydrogen bond between the amide and the carboxylate groups, but such an interaction, which requires a deviation from the NH *anti* orientation, is likely not frequently populated in water solution (Blundell, DeAngelis, & Almond, 2006). Nonetheless, a recent study demonstrated that under acidic conditions, a strong inter-chain hydrogen-bond structure involving amide and carboxylate groups of adjacent residues appeared (Giubertoni, Burla, et al., 2019). Due to this possibility, it remains unclear whether the amide proton takes part in hydrogen bonds to a large extent and whether it deviates from the *anti* conformation. Our previous NMR spectroscopic studies suggested that NOEs involving the amide proton in the HA polymer were not consistent with a normal *anti* conformation in relation to the adjacent ring proton, which indicates the possible presence of a *syn* conformation between H2

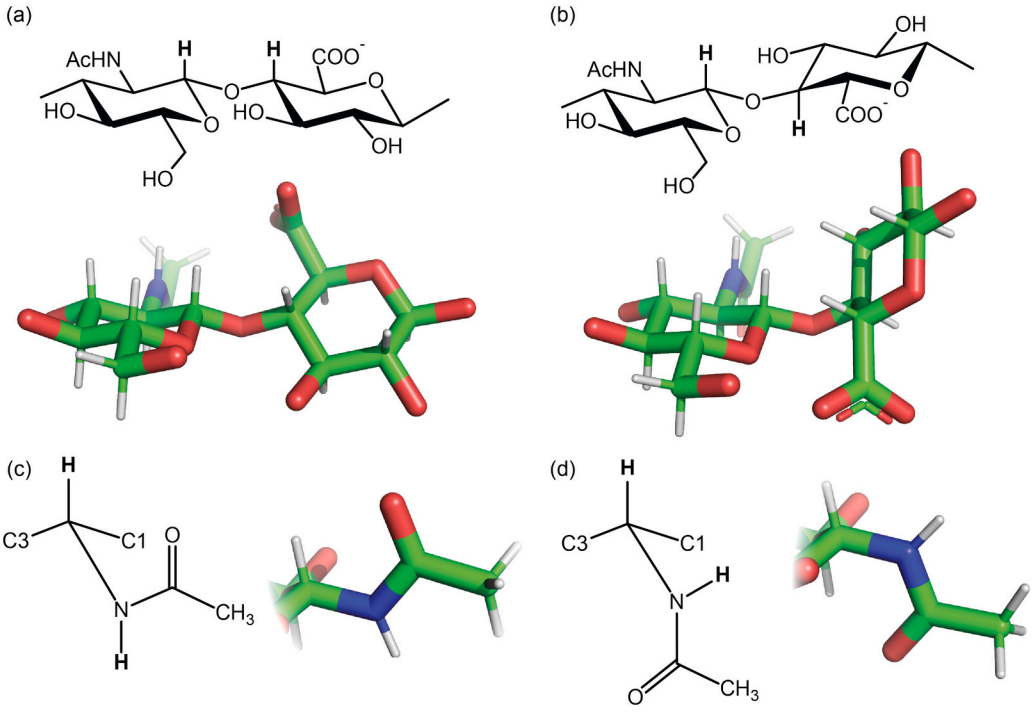

Fig. 2. Schematic representations of (a) standard *syn* conformation of $\beta(1 \rightarrow 4)$ glycosidic linkage; (b) minor *anti* conformation of $\beta(1 \rightarrow 4)$ glycosidic linkage after a flip; (c) normal *anti* conformation of the *N*-acetyl group; (d) minor *syn* conformation of the *N*-acetyl group.

and NH (Fig. 2d) (Nestor & Sandström, 2017). This possible amide *syn* conformation in HA polysaccharides is not consistent with the average model presented by Almond et al. (2006). Meanwhile, about 2 % of *syn* conformation between H2 and NH of β-GlcNAc monosaccharide was also predicted (Xue & Nestor, 2022). Whether such a conformation occurs in more rigid and longer HA chains is still unknown.

As mentioned previously, HA_8 has been extensively investigated by NMR spectroscopy to mimic the conformation of HA polymers in aqueous solution (Almond et al., 2006; Blundell, DeAngelis, & Almond, 2006; Cowman et al., 1984; Nestor et al., 2010). However, few studies have focused on more detailed comparisons between HA_8 and longer HA chains. A recent MD study suggested that the conformational landscape from GAG 20-mer likely provides a better representation of conformations of long GAG polymers than existing conformational landscapes of monosaccharides and oligosaccharides (Whitmore et al., 2020). We hypothesize that a detailed NMR analysis of a 20-mer of HA (HA_{20}) can provide a more accurate model of the HA polymer than the previous NMR studies on HA_8.

Here we present our study on HA_8 and HA_{20} by NMR spectroscopy to investigate the conformational changes between different chain lengths of HA. A series of NMR experiments were performed to measure NOEs and coupling constants under different conditions to provide more detailed information about the HA structure, with a special focus on the conformation of the glycosidic linkages and the *N*-acetyl group of GlcNAc.

2. Experimental

2.1. Nomenclature

The HA oligomers are abbreviated HA_x where x refers to the number of monosaccharide residues in the chain. Protons are referred to as N_y ($GlcNAc_y$) and G_y ($GlcA_y$) where y indicates the proton position on the pyranosyl ring. The glycosidic linkages were defined by two dihedral angles: φ (H_1-C_1-O_z-C_z) and ψ (C_1-O_z-C_z-H_z) respectively, where z depends on the linkage (3 or 4).

Syn and *anti* conformations of glycosidic linkages were defined based on the difference between the two torsion angles, φ and ψ. Specifically, a difference of $0^\circ \pm 90^\circ$ corresponds to the *syn* conformation, while a difference of $180^\circ \pm 90^\circ$ corresponds to the *anti* conformation according to the IUPAC nomenclature (Cross & Klyne, 1976; Klyne & Prelog, 1960). In practice, this means that the protons at the glycosidic linkage (H_1 and H_z) are on the same side of the glycosidic linkage in *syn* conformations and on opposite sides in *anti* conformations.

The *N*-acetyl group was defined by two torsion angles: θ_1 (H2-C2-N-NH) and θ_2 (C2-N-CO-CH_3). *Syn* and *anti* conformations correspond to $\theta_1 = 0^\circ$ and $\theta_1 = 180^\circ$, respectively. The amide bond, defined by θ_2, is considered a predominant *trans* ($\theta_2 = 180^\circ$) conformation in this study.

2.2. Sample preparation

2.2.1. Degradation

HA polysaccharide (hyaluronic acid sodium salt in powder form from *Streptococcus equi* bacteria, a gift from Galderma, Uppsala, Sweden; Mw 400 kDa) solution (5 ml, 30 mg/ml) was degraded by treatment with bovine testicular hyaluronidase (5 ml, 5968 units/ml) (CAS Number 37326-33-3, Sigma Aldrich) in 0.2 M NaCl solution at pH 4.4 overnight at 37 °C and the reaction was terminated by boiling for 15 min. The digest was lyophilized and dissolved in 50 mM NaCl buffer solution at pH 4.0. The solution was centrifuged at 30,000 rpm for 5 min and the supernatant was collected for fractionation by HPLC.

2.2.2. Separation

The mixture of HA oligosaccharides was separated by ion-exchange chromatography using a SAX-HPLC preparative column (column dimensions: 150 mm × 20 mm, using HYPERSIL GOLD SAX™ as packing material with particle size of 5 μm). The separation was performed after 1 ml sample injection by using eluent A (50 mM NaCl solution at pH 4.0) for 5 min followed by a linear gradient from 100 % eluent A to 100 % eluent B (1.2 M NaCl solution at pH 4.0) for another 5–60 min, with 1.2 ml/min flow rate and 214 nm UV detection (Fig. S1) (Volpi, 2007). All fractions were collected automatically and further concentrated by speed vacuum centrifugation at 1500 rpm at 25 °C and then lyophilized.

The obtained powder from the fractions containing HA_8 and HA_{20} were each dissolved in 1 ml, 0.1 M ammonium acetate pH 7.8 and then further purified from salt and other contaminations by size-exclusion chromatography. A sample loop (1 ml) was used for injection on an ÄKTA system consisting of a Sephadex G-10 column (GE Healthcare, Uppsala, Sweden), a P-900 pump, a UV-900 detector, and a Frac-900 fraction collector. Isocratic elution with 0.1 M ammonium acetate pH 7.8 at a 1.5 ml/min flow rate was used and the eluates were monitored under 214 nm, 260 nm, and 310 nm UV detection, and fractions were collected automatically based on the UV signals.

The pure fractions containing HA_8 and HA_{20} were lyophilized for at least 24 h to eliminate ammonium acetate contamination. The HA oligomers were further loaded on a Dowex 50WX8 cation exchange column in its H^+ form to remove ammonium ions and to obtain the samples in its protonated form. The column was made from a disposable glass Pasteur pipette packed with the cation exchange resin with a small plug of glass wool at the outlet. Before loading the sample, the resin was activated by 100 mM HCl followed by flushing with Milli-Q® water until discoloration of the eluate disappeared and pH went back to neutral. The samples were dissolved in 600 μl Milli-Q® water, loaded on the column and fractions were collected by elution with Milli-Q® water. Fractions containing HA were pooled and pH was adjusted to 7.0 with 100 mM NaOH, producing the sodium salt of HA. The fractions were lyophilized for further NMR analysis.

2.3. NMR spectroscopy

HA_8 and HA_{20} samples were dissolved in either 90 % H_2O/10 % D_2O or D_2O (600 μl) respectively, to obtain one HA_8 (11 mM) and one HA_{20} sample (8 mM). The pH of the samples was fine-tuned to 7.0 ± 0.2 with HCl or NaOH solutions. Given an almost complete dissociation of HA carboxylate groups at pH 7.0 (pK_a of 3.0), the final sodium ion concentration was close to 44 and 80 mM, respectively, for the HA_8 and HA_{20} samples. The sample was transferred into a 5 mm NMR sample tube for further analysis.

NMR spectra were recorded at either 5 °C or 25 °C on a Bruker Avance III 600 MHz spectrometer using a 5 mm $^1H/^{13}C/^{15}N/^{31}P$ inverse detection CryoProbe equipped with a z-gradient. $^1H,^{13}C$-HSQC-NOESY and $^1H,^{13}C$-HSQC-ROESY spectra from the Bruker pulse sequence library (*hsqcetgpnosp* and *hsqcetgprosp*, respectively) were recorded with 1 k data points in t_2 and 256 increments in t_1 using 64 scans per increment and a relaxation delay of 1.5 s. For each sample, eleven $^1H,^{13}C$-HSQC-NOESY spectra were recorded with mixing times (τ_m) ranging from 20 to 300 ms, whereas one $^1H,^{13}C$-HSQC-ROESY spectrum was recorded with τ_m of 200 ms.

Heteronuclear long-range *J*-HMBC spectra (Willker & Leibfritz, 1995) were recorded with 2 k data points in t_2 and 256 increments in t_1 using 32 scans per increment and a relaxation delay of 1.5 s. The maximum evolution time τ_{max} was set to 200 ms and 150 ms for HA_8 and HA_{20} respectively, and 10 spectra were recorded with evolution times (τ_m) ranging from 20 to 198 ms for HA_8 and from 10 to 148 ms for HA_{20}. Constant-time *J*-HMBC spectra (Bruker pulse sequence *hmbcetgpjcl2nd*), where long-range couplings can be measured directly from the indirect dimension of the spectra, were also recorded (Meissner & Sørensen, 2001). Three spectra were recorded on each sample with a scaling factor (κ) of 21–53, 2k data points in t_2 and 128–500 increments in t_1 using 32 scans per increment and a relaxation delay of 1.5 s. The coupling evolution delay was set to 250 ms in all constant-time *J*-HMBC experiments. NMR spectra were processed with TopSpin 4.0.6 (Bruker). The same

integral areas and processing parameters were used for each spectrum under the same experimental condition.

2.3.1. Calculation of interproton distance

The $^{1}H,^{13}C$-HSQC-NOESY mixing time series (20–300 ms) were evaluated by using the Peak Amplitude Normalization for Improved Cross-relaxation (PANIC) approach (Hu & Krishnamurthy, 2006; Kolmer et al., 2015; Macura et al., 1986). Using this approach, each NOE cross-peak is normalized within the same spectrum to cancel out the nonlinear component in the NOE buildup curves according to Eq. (1):

$$a_{\text{normalized volume}} = \frac{a_{AB}}{(n_B a_{AA} + n_A a_{BB})/2} \quad (1)$$

where a_{AB} is the NOE cross-peak, a_{AA} and a_{BB} are the diagonal peaks, and n_A and n_B are the number of protons. The PANIC approach yields linear build-up curves where the cross-relaxation rate is obtained from the slope of the curve by simple linear regression. The isolated spin-pair approximation was used to obtain distances from cross-relaxation rates:

$$r_{IS} = r_{ref}\left(\frac{\sigma_{IS}}{\sigma_{ref}}\right)^{-\frac{1}{6}} \quad (2)$$

where r_{IS} is the distance between proton I and S, and σ_{IS} is the cross-relaxation rate. Distances are obtained by calibration of the cross-relaxation rates against an internal distance standard, i.e. r_{ref}, with σ_{ref} being the cross-relaxation rate of the reference distance. As reference distance, G_1–G_3 was chosen and the reference distance was set to 2.56 Å based on an average structure model of HA_8 (Almond et al., 2006). Only the buildup curves that exhibited a coefficient of determination (R^2) equal to or greater than 0.95 were chosen for the subsequent calculation of interproton distances. Each build-up curve included a minimum of 8 data points (Figs. S2 and S3).

2.3.2. Calculation of heteronuclear coupling constants

The long-range proton-carbon coupling constants over the glycosidic linkages and within the *N*-acetyl group were measured quantitatively by a series of gradient-selected *J*-HMBC experiments with increasing coupling evolution time τ_m. The signal amplitude of the cross-peaks showed a characteristic sinusoidal dependence and accurate J_{CH} coupling constants could be obtained by fitting the ideal sinusoidal curve to the experimental data (Figs. S4 and S5) (Willker & Leibfritz, 1995):

$$I = k \times \sin(\pi \times J_{CH} \times \tau_m) \quad (3)$$

where I is the intensity of the integration values and k is the scaling factor.

Coupling constants from constant-time *J*-HMBC spectra were measured from 1D projections of the resonances of interest, utilizing the splitting by $\kappa \times {}^{n}J_{CH}$ in the f1 dimension.

2.3.3. The acetamido group

Starting from the HA_8 model predicted by Almond et al. (2006) (Protein Data Bank accession code: 2BVK), the torsion angle θ_1 was incremented by 1° within the range of −180° to −140° and 160° to 180°, and the angle was incremented by 10° within the range of −140° to 160°, resulting in a total of 90 different angles. A list of the corresponding interproton distances of NH-H_1, NH-H_2, and NH-H_3 was generated at each angle.

Furthermore, two coupling constants $^{3}J_{H2\text{-}NH}$ and $^{3}J_{H2\text{-}CO}$ were also calculated based on parameterized Karplus equations within the range of −180° to 180° (Hu, Carmichael, & Serianni, 2010):

$$^{3}J_{H2-NH} = 5.08 - 0.83\cos\alpha + 5.02\cos(2\alpha) + 0.03\sin\alpha + 0.06\sin(2\alpha) \quad (4)$$

$$^{3}J_{H2-CO} = 3.11 - 2.02\cos\alpha + 2.88\cos(2\alpha) - 0.04\sin\alpha + 0.05\sin(2\alpha) \quad (5)$$

where α is the H2-C2-N-NH torsion angle (equivalent to θ_1) for $^{3}J_{H2,NH}$ and the H2-C2-N-CO torsion angle for $^{3}J_{H2\text{-}CO}$.

2.3.4. The glycosidic linkages

In the 2BVK model, the two torsion angles φ and ψ at the glycosidic linkages were simultaneously rotated in 10° increments from −180° to 180°, resulting in 1369 (37 × 37) combinations, and the θ_1 torsion angle of GlcNAc was correspondingly kept at the most probable angle previously determined. A list of the corresponding interproton distances (G_1-N_2, G_1-N_3, G_1-NH, G_1-N_4, G_2-N_2 for the $\beta(1 \rightarrow 3)$ linkage and N_1-G_4, N_1-G_3, N_1-G_5 for the $\beta(1 \rightarrow 4)$ linkage) was generated from each combination of φ and ψ. The procedure was repeated with 1° increments around the global minima of φ and ψ.

$^{3}J_{N(C3)\text{-}G(H1)}$ and $^{3}J_{G(C4)\text{-}N(H1)}$ were calculated based on the parameterized Karplus equation related to the torsion angle φ within the range of −180° to 180° (Säwén et al., 2010):

$$^{3}J_{CH}(\varphi) = 6.54\ cos^2(\varphi - \Delta) - 0.62\ cos(\varphi - \Delta) - 0.17 \quad (6)$$

where $\Delta = +12°$ for β-D-hexopyranosides.

3. Results and discussion

3.1. Isolation of HA

HA polysaccharide was enzymatically degraded with hyaluronidase as previously described (Chen et al., 2009; Gold, 1982) and the product mixture was separated by anion exchange chromatography (Fig. S1). The fractions with even-numbered HA chains (HA_8 and HA_{20}) possessed $\beta(1 \rightarrow 3)$ glycosidic linkages at both termini, which corresponds to the degradation pattern shown by testicular hyaluronidase (Weissmann et al., 1954). HA_8 and HA_{20} were dissolved in 90 % H_2O/10 % D_2O as well as in pure D_2O for NMR analysis at both 5 and 25 °C.

3.2. Interproton distances and J-couplings

To address the conformation of the glycosidic linkages and *N*-acetyl groups of HA with different chain lengths, NMR observables were measured, in particular, interproton distances from ^{1}H cross-relaxation rates, and three-bond hetero- and homonuclear coupling constants. Inter-residue NOEs between GlcA and GlcNAc are particularly useful to define the geometry of the glycosidic linkages due to the absence of large *J*-couplings. Of the two major side groups, the carboxylate on GlcA and the acetamido group on GlcNAc, only the conformation of the latter can be defined by proton NOEs and *J*-couplings ($^{3}J_{HH}$ and $^{3}J_{CH}$) (Holmbeck et al., 1994). However, $^{1}H,^{1}H$-NOESY spectra can only provide limited information because of the severe overlap of proton signals in the medium-sized sugar molecules, which makes the analysis of proton distance challenging. Previous studies utilizing $^{1}H,^{1}H$-NOESY spectra on HA oligosaccharides have been hampered by these challenges, especially over the glycosidic linkages, since the spectral overlap between N_3, G_4 and G_5 cannot be fully resolved (Donati et al., 2001; Holmbeck et al., 1994; Nestor et al., 2010). To avoid such a problem, 2D $^{1}H,^{13}C$-HSQC-NOESY experiments were recorded in this study, which takes advantage of the larger spectral dispersion in the carbon dimension and can achieve an unambiguous assignment by alleviating signal overlap. In this NMR experiment, the important inter-residue NOEs that convey conformational information appear well separated in the carbon dimension as shown in Fig. 3a–c. Furthermore, to demonstrate the well-dispersed carbon resonances, the corresponding HSQC spectrum is also shown in Fig. 3d. Resonances that have similar proton chemical shifts (such as N_3/G_4/G_5) are well separated in the carbon dimension, thus, NOE cross-peaks can be used directly to determine the inter-proton distances without subtraction of overlapping cross-peaks.

When analysing NOEs, the presence of relayed NOEs may affect the results considerably, especially with long mixing times (Bax et al.,

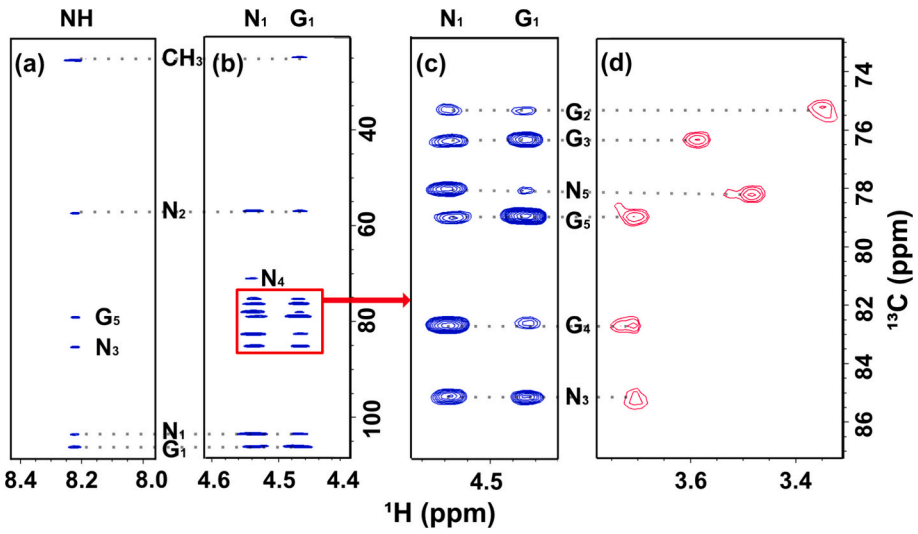

Fig. 3. Selected regions of 2D NMR spectra showing the interior residues of HA_{20} (8 mM in 90 % H_2O/10 % D_2O at 5 °C, mixing time (τ_m) = 0.3 s): (a) ^1H,^{13}C-HSQC-NOESY spectrum of the GlcNAc amide proton region; (b) and (c) ^1H,^{13}C-HSQC-NOESY spectrum of the anomeric proton region; (d) corresponding cross-peaks in the ^1H,^{13}C-HSQC spectrum.

1986). This effect, also known as spin diffusion, is caused by a third proton C in close proximity to the two protons A and B, which will affect the measured distance r_{AB} by a relayed or two-step NOE pathway from A via C to B. Several examples of relayed NOEs were observed from the HSQC-NOESY spectra. For example, the G_2-N_1 NOE in Fig. 3c is most probably due to a relayed NOE via G_4. In order to avoid NOEs with significant contribution of spin diffusion, ^1H,^{13}C-HSQC-ROESY spectra were recorded, where direct NOE cross-peaks are always of the opposite sign compared to the diagonal/HSQC cross-peaks, whereas cross-peaks due to spin diffusion are of the same sign or too weak to be detected (Bax et al., 1986). Thus, only NOE cross-peaks with the correct sign in HSQC-ROESY spectra were used for further analysis (Fig. S6). In addition, the linearity of the NOE build-up curves were investigated and NOEs from long mixing times with deviations from the linear shape were omitted.

Since the ^1H and ^{13}C chemical shifts of the interior residues (GlcNAc and GlcA, respectively) are either identical or very similar in HA_8 and HA_{20}, proton distances were measured as an average over all interior residues in this study.

In addition, $^3J_{CH}$ were obtained from long-range *J*-HMBC spectra (Fig. S7) and $^3J_{HH}$ were obtained from 1D ^1H NMR spectra (Fig. S8) to determine the dihedral angles of the glycosidic linkages and the acetamido group. However, due to spectral overlap and/or small coupling constants, only one $^3J_{CH}$ from each glycosidic linkage could be determined ($^3J_{N(C3)\text{-}G(H1)}$ and $^3J_{G(C4)\text{-}N(H1)}$), as well as one from the *N*-acetyl group ($^3J_{H2\text{-}CO}$).

In order to perform an unbiased analysis of the NMR data, we decided to start from NMR data only without any input from MD simulations or similar. Using simple analysis of each torsion angle, we could estimate their values based on NOEs and *J*-couplings. The results were then compared to other experimental and computational studies. When a single conformation was not enough to explain the NMR data, we used input from previous computational studies to generate a conformational ensemble.

3.3. Conformation of the acetamido group

Torsion angle θ_1 of the acetamido group is used to assess the conformation of the flexible C2-N2 bond, in which H2 and NH are generally considered to be in an *anti* orientation in both GlcNAc monosaccharide and HA oligosaccharides (Blundell, DeAngelis, & Almond, 2006; Donati et al., 2001; Hu, Zhang, et al., 2010). As shown in Fig. 3a, most of the strong NOE cross-peaks to NH originate from the neighboring positions in GlcNAc (N_1, N_2, N_3 and CH_3), of which NH-N_1, NH-N_2, and NH-N_3 were used for conformational analysis. Together with two *J*-couplings ($^3J_{H2\text{-}NH}$ and $^3J_{H2\text{-}CO}$) that are sensitive to the θ_1 torsion angle, the five sets of experimental data were used to determine the geometry of the acetamido side group in HA_8 and HA_{20} (Table 1).

Our experimental interproton distances are in good agreement with the predicted distances from MD simulations (Almond et al., 2006) and from earlier NMR studies (Donati et al., 2001; Holmbeck et al., 1994). The two *J*-couplings are also consistent with values derived from the GlcNAc monosaccharide, showing an *anti* conformation of the *N*-acetyl side group (Xue & Nestor, 2022).

The absolute differences between our NMR data (Table 1) and calculated distances and *J*-couplings from the model structure were used to obtain the root mean square deviation (RMSD) across the entire torsion angle span. Minimization plots were generated, where the global minimum corresponds to the most probable value of the torsion angle θ_1 (Fig. S9). The global minima for HA_8 and HA_{20} were found at (165 ± 6)° and (−167 ± 13)°, respectively, which represents the average structure and is close to 180°, equivalent to a strict *anti* conformation. Thus, the orientation of the *N*-acetyl group is very similar in HA_8 and HA_{20}, which is consistent with earlier conclusions from NMR studies on HA oligo- and polysaccharides (Blundell, DeAngelis, & Almond, 2006; Cowman et al., 1984). The results suggest a slight tilt of NH towards N_3 in HA_8 and towards N_1 in HA_{20}, but it

Table 1
Interproton distances (Å) and *J*-couplings (Hz) that are sensitive to the torsion angle θ_1.

		NH-N_1	NH-N_2	NH-N_3	$^3J_{H2\text{-}NH}$	$^3J_{H2\text{-}CO}$[a]
Experimental	HA_8[b]	2.8 ± 0.1	2.9 ± 0.1	2.6 ± 0.1	10.4 ± 0.1	3.6 ± 0.3[c]; 3.5 ± 0.3[d]
	HA_{20}[b]	2.7 ± 0.1	3.0 ± 0.1	2.8 ± 0.1	10.1 ± 0.1	2.8 ± 0.1[d]; 2.9 ± 0.2[d]
Calculated	HA_8[e]	2.7	3.0	2.4	10.2	3.6
	HA_{20}[e]	2.5	3.0	2.6	10.4	3.7

[a] *J*-couplings from *J*-HMBC; CT-*J*-HMBC experiments.
[b] At 5 °C in 90 % H_2O/10 % D_2O.
[c] At 5 °C in D_2O.
[d] At 25 °C in D_2O.
[e] Calculated interproton distances from the model structure and coupling constants from the parameterized Karplus equations after adjusting the torsion angle θ_1 to the global minimum.

should be noted that the data is averaged over several residues, so there may be differences along the chain. Also, the obtained average conformations do not exclude the presence of minor conformations, but the excellent fit between experimental and calculated data suggests that the major *anti* conformation is predominant. Any significant differences from this conformation with sufficient lifetime would be observed as a shorter H2-NH distance and with differences in the coupling constants. The only clear difference between experimental and calculated data is observed for $^{3}J_{H2\text{-}CO}$ of HA_{20} (2.8–2.9 Hz from NMR data and 3.7 Hz from the parametrized equation). However, the parametrized Karplus equation was derived from the GlcNAc monosaccharide with an implicit water model, which may not accurately mimic the real water-solute interactions (Hu, Carmichael, & Serianni, 2010). The glycosidic linkages on GlcNAc C_1 and C_3, dynamics of the GlcNAc ring and the nearby sodium ion could all affect the magnitude of the coupling constant compared to the calculated value.

The torsion angle corresponding to the global minimum for each condition was applied to subsequent glycosidic linkage calculations to ensure that differences in the acetamido group conformation were included.

3.4. Conformation of the β(1 → 3) glycosidic linkage

Three interproton distances (G_1-N_2, G_1-N_3, G_1-NH) and one *trans*-glycosidic coupling constant ($^{3}J_{N(C3)\text{-}G(H1)}$) were obtained from NMR experiments to investigate the conformation of the β(1 → 3) glycosidic linkage. NOEs from G_1-N_3 and G_1-NH have previously been observed in short HA oligosaccharides (Almond et al., 2006; Donati et al., 2001; Holmbeck et al., 1994; Nestor et al., 2010). These two NOEs support the *syn* conformation over the glycosidic linkage and are in agreement with the *exo*-anomeric effect. Another NOE from G_1-N_2 has earlier been observed in both NOESY and ROESY spectra and was considered as "a genuine cross-peak" with little effect from spin diffusion (Donati et al., 2001; Nestor et al., 2010). In addition, two interproton distances, G_1-N_4 and G_2-N_2, were set to be longer than 4 Å, as they did not show any NOE correlation in the ^{1}H,^{13}C-HSQC-NOESY spectra.

Similar to the torsion angle θ_1, our experimental results (Table 2) were further compared with distances and *J*-couplings obtained from the model structure. RMSDs between experimental and modeled data were calculated based on five interproton distances and one *J*-coupling and minimization diagrams were plotted as shown in Figs. 4 and S10.

The heatmaps show the (φ, ψ) distribution of the β(1 → 3) glycosidic linkage for HA_8 and HA_{20}, respectively. The global minimum of (φ_{13}, ψ_{13}), corresponding to the smallest deviation between the experimental NMR data and the computed model, is located at ((46 ± 6)°, (15 ± 9)°) for HA_8 (Figs. 4a and S10a). This result is close to the MD simulation results from HA_4 and HA_6 reported by Almond et al. (2006) with average (φ_{13}, ψ_{13}) angles of (50.7°, 9.7°). All the currently reported data on glycosidic linkage torsion angles of HA in solution are from MD simulations, which require the inclusion of explicit water models in the simulations (Guvench, 2022). However, choosing the most reliable water model is not straightforward because differences between these models may generate differences in solute-solvent interactions, which then propagate to differences in solute behavior (Florová et al., 2010). Previous simulations including explicit water models gave generally consistent values of φ_{13}, typically between 46° and 52°, but values of ψ_{13} display significant variation, spanning from −10° to 25° (Almond et al., 2006; Donati et al., 2001; Gargiulo et al., 2010; Holmbeck et al., 1994; Kaufmann et al., 1998; Taweechat et al., 2020; Whitmore et al., 2020). Our results are purely based on NMR data and provide experimental support to the β(1 → 3) conformation established by MD simulations.

As can be seen in Table 2, the G_1-N_3 distance was slightly longer in HA_{20} compared to HA_8, accompanied by a slightly shorter G_1-N_2 distance. This difference propagates into an altered conformation of the glycosidic linkage with (φ_{13}, ψ_{13}) angles of ((51 ± 7)°, (35 ± 18)°) for HA_{20} as shown in Figs. 4b and S10b. The theoretical and experimental values agree very well, where the values of HA_{20} are almost identical. This consistency supports the presence of a predominant conformation of the β(1 → 3) glycosidic linkage without significant contribution of minor conformations.

Importantly, the minimization plots (Fig. 4) are single-state models and can only be used to target the global minimum conformation as long as minor conformations are not populated to a significant amount. Minima other than the global minimum do not represent minor populations since no steric restraints were added or energy minimizations were performed. Thus, the second minima in Fig. 4 at (−20°, 30°) and (−20°, 60°) for HA_8 and HA_{20}, respectively, are not representative of minor populations. Recent MD simulations have found minor populations at (φ_{13}, ψ_{13}) angles of (65°, −149°) (Whitmore et al., 2020) and (62°, −143°) (Lutsyk & Plazinski, 2021), but with free energies of 13–15 kJ/mol compared to the global minimum. This is equivalent to a minor population of <1 %, which would be very difficult to detect with our NMR methods.

3.5. Conformation of the β(1 → 4) glycosidic linkage

Three interproton distances (N_1-G_4, N_1-G_3, N_1-G_5) and one *trans*-glycosidic coupling constant ($^{3}J_{G(C4)\text{-}N(H1)}$) were obtained from the NMR analysis to investigate the conformation of the β(1 → 4) glycosidic linkage (Table 3). The short N_1-G_4 distances obtained from HA_8 and HA_{20}, which are equivalent to the expected *syn* conformation over the glycosidic linkage, are almost identical to the distance from the previous MD model (Almond et al., 2006). However, the N_1-G_3 distance obtained from HA_{20} and the N_1-G_5 distance obtained from HA_8 and HA_{20} are much shorter than predicted from the model. No NOE was observed between N_1 and G_5 from HA_8, resulting in only two NOEs and one *J*-coupling for analysis of the β(1 → 4) glycosidic linkage conformation. This did not provide enough data for building a model based on NMR data only, especially since the *J*-coupling is sensitive to only one of the two dihedral angles.

Table 2
Interproton distances (Å) and one *trans* glycosidic *J*-coupling (Hz) that are sensitive to the conformation of the β(1 → 3) glycosidic linkage.

		G_1-N_3	G_1-N_2	G_1-NH	G_1-N_4	G_2-N_2	$^{3}J_{N(C3)\text{-}G(H1)}$ [a]
Experimental	HA_8	2.5 ± 0.1 [b]	3.4 ± 0.1 [b]	2.6 ± 0.1 [c]	>4 [f]	>4 [f]	3.9 ± 0.2 [d]; 4.1 ± 0.1 [e]
	HA_{20}	2.7 ± 0.1 [b]	3.2 ± 0.1 [b]	2.5 ± 0.1 [c]	>4 [f]	>4 [f]	3.3 ± 0.3 [e]; 3.3 ± 0.2 [e]
Calculated	HA_8 [g]	2.3	3.6	2.3	4.4	4.8	3.8
	HA_{20} [g]	2.6	3.2	2.5	4.4	4.8	3.3

[a] *J*-couplings from *J*-HMBC; CT-*J*-HMBC experiments.
[b] At 5 °C in 90 % H_2O/10 % D_2O and D_2O.
[c] At 5 °C in 90 % H_2O/10 % D_2O.
[d] At 5 °C in D_2O.
[e] At 25 °C in D_2O.
[f] Distances were set to be longer than 4 Å.
[g] Calculated interproton distances from the model structure and coupling constants from the parameterized Karplus equations after adjusting the torsion angles φ and ψ to the global minima.

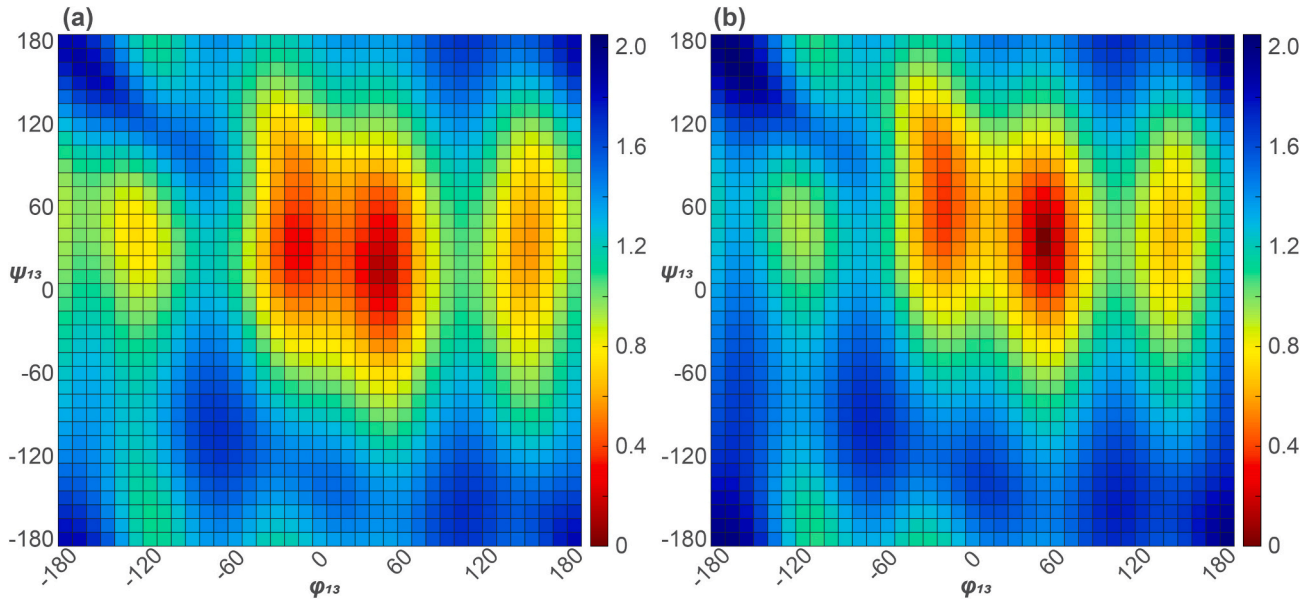

Fig. 4. Conformational heatmaps showing the (φ, ψ) distribution with 10° × 10° bins of the $\beta(1 \rightarrow 3)$ glycosidic linkage of (a) HA_8 and (b) HA_{20}. Colors indicate the RMSD values ranging from highest (blue) to lowest (red).

Table 3
Interproton distances (Å) and one *trans* glycosidic *J*-coupling (Hz) that are sensitive to the conformation of the $\beta(1 \rightarrow 4)$ glycosidic linkage.

		N_1-G_4	N_1-G_3	N_1-G_5	$^3J_{G(C4)\text{-}N(H1)}$[a]
Experimental	HA_8	2.2 ± 0.1[b]	2.8 ± 0.1[b]	abs.	3.5 ± 0.2; 3.3 ± 0.3[c]
	HA_{20}	2.4 ± 0.1[b]	2.7 ± 0.1[b]	2.8 ± 0.1[b]	n.d.; 3.5 ± 0.2[c]
Calculated[d]	HA_8	2.3	4.4	3.9	3.6

[a] *J*-couplings from *J*-HMBC; CT-*J*-HMBC experiments.
[b] At 5 °C in 90 % H_2O/10 % D_2O and D_2O.
[c] At 5 °C in D_2O.
[d] Interproton distances and calculated coupling constant from the parameterized Karplus equation based on the model structure (φ_{14}, ψ_{14}) = (47.9°, 8.0°); abs. = absence; n.d. = not determined.

An attempt was made to build a model from the three NOEs and one *J*-coupling from HA_{20}. However, the heatmap based on RMSDs between experimental and theoretical data did not show a well-defined global minimum, with all RMSDs >0.5 (Fig. S11). The lack of consistency between theoretical and experimental values show that the experimental data do not support the presence of one predominant conformation over the $\beta(1 \rightarrow 4)$ glycosidic linkage. Instead, it suggests that two or more different conformations coexist over the $\beta(1 \rightarrow 4)$ glycosidic linkage.

To explore the correlation between the NMR data and various conformations, we employed the conformations derived from the MD simulation conducted by Whitmore et al. (2020) on HA_{20}. Their study assessed the $\beta(1 \rightarrow 4)$ glycosidic linkage based on Gibbs free energy ΔG (φ_{14}, ψ_{14}) minima and revealed one global minimum (conformation I: ΔG = 0 kcal/mol) along with two additional local minima (conformation II: ΔG = 1.31 kcal/mol and conformation II′: ΔG = 1.42 kcal/mol). The global minimum conformation I (φ_{14}, ψ_{14}) = (50.0°, −3.1°) (Fig. 5a) is similar to the MD simulation data reported by Almond et al. (2006) with average (φ_{14}, ψ_{14}) angles of (47.9°, 8.0°). The two minor conformations II and II′ are *anti* conformations located at (φ_{14}, ψ_{14}) = (35.0°, 167.0°) and (φ_{14}, ψ_{14}) = (60.0°, −153.1°), respectively (Fig. 5b and c). The calculated interproton distances and ^3J coupling constant based on each of these conformations are presented in Table 4. Comparison of these three conformations with the NMR data further confirmed the existence of an equilibrium between major and minor conformations across the $\beta(1 \rightarrow 4)$ glycosidic linkage. Therefore, the expected ratio between the conformations at 5 °C was calculated based on the reported ΔG of each conformation, and was determined to be 83 %, 9 %, and 8 %, respectively. The ratio of each conformation was taken into account, leading to further calculations of the weighted interproton distances and ^3J coupling constant (Table 4). The calculated interproton distances show a maximum deviation of 0.2 Å from the experimental data of HA_{20} (Table 3), suggesting that the experimental results are in good agreement with this conformation distribution ratio.

Furthermore, by adjusting the distribution ratio of the three conformations, a ratio that best fits the HA_8 experimental data was found. This ratio consists of 92 % conformation I and 8 % conformation II′, where the calculated interproton distances and ^3J-couplings are almost identical to the experimental data. In addition, the weighted interproton distance of N_1-G_5 was calculated to be 4.0 Å, thus further supporting the reason for the absence of the N_1-G_5 NOE cross-peaks in the ^1H,^{13}C-HSQC-NOESY spectra of HA_8.

Fig. 5 clearly illustrates that the two *anti* conformations display significantly shorter interproton distances for N_1-G_3 and N_1-G_5 compared to the *syn* conformation. This observation explains the discrepancy between the experimental data and the calculated values based on the assumption of a 100 % *syn* conformation. In both HA_8 and HA_{20}, conformation I stands out as the predominant conformation, and both chain lengths are predicted to populate 8 % of conformation II′. However, HA_{20} exhibits an additional 9 % of conformation II, which is absent in HA_8. Our findings provide the first experimental support for an equilibrium between *syn* and *anti* conformations over the $\beta(1 \rightarrow 4)$ conformation, previously predicted by MD simulations.

Anti conformations or "flipped" conformations over the $\beta(1 \rightarrow 4)$ linkage induced by Na^+ interactions have recently been associated with distinct hairpin-like structures that are observed in MD simulations (Kutálková et al., 2020). With the amount of *anti* conformation predicted from our NMR data (8 % in HA_8 and (9 + 8)% in HA_{20}), on average one out of four HA_8 molecules has a $\beta(1 \rightarrow 4)$ linkage in *anti* conformation since one HA_8 has three $\beta(1 \rightarrow 4)$ linkages ($1/(4 \bullet 3\ \beta(1 \rightarrow 4)$ linkages) = 0.08). For HA_{20}, on average 1.5 $\beta(1 \rightarrow 4)$ linkages in each molecule are in *anti* conformation since one HA_{20} has nine $\beta(1 \rightarrow 4)$ linkages (1.5/(9 $\beta(1 \rightarrow 4)$ linkages) = 0.17). According to previous MD simulations, these *anti* conformations are short-lived, in the order of tens of nanoseconds (Kutálková et al., 2020), which could explain why we do not observe

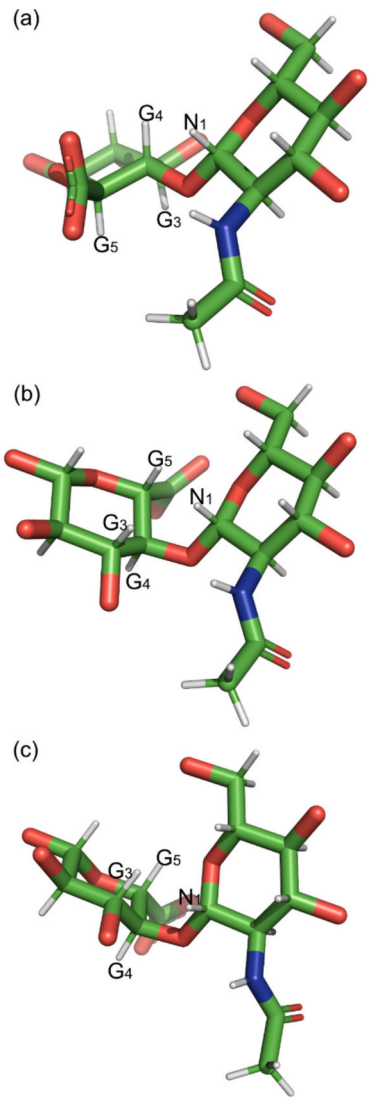

Fig. 5. Schematic representations of three possible conformations of the $\beta(1 \rightarrow 4)$ glycosidic linkage: (a) conformation I with *syn* conformation between N_1 and G_4; (b) conformation II with *anti* conformation between N_1 and G_4; (c) conformation II′ with *anti* conformation between N_1 and G_4.

Table 4
Three minimal conformations from MD simulations (Whitmore et al., 2020) and two weighted ratios, along with their corresponding interproton distances (Å) and ^3J-couplings (Hz).

Conformation	Percentage (%)			N_1-G_4	N_1-G_3	N_1-G_5	$^3J_{G(C4)\text{-}N}$ (H1)
	I	II	II′				
MD simulation[a]	100	0	0	2.2	4.4	4.0	3.4
	0	100	0	3.6	1.9	2.1	4.8
	0	0	100	3.4	1.8	3.5	2.3
Weighted	83	9	8	2.3	2.5	3.0	3.4
calculation	92	0	8	2.2	2.8	4.0	3.3

[a] In the MD simulation, the dihedrals were defined as φ (O_5-C_1-O_4-C_4) and ψ (C_1-O_4-C_4-C_3). For conversion to our definition, φ (H_1-C_1-O_4-C_4) = φ (O_5-C_1-O_4-C_4) +118.7° and ψ (C_1-O_4-C_4-H_4) = ψ (C_1-O_4-C_4-C_3) −119.3°.

separate chemical shifts from these conformations. However, since they populate a significant amount of the $\beta(1 \rightarrow 4)$ linkages, they will still affect the measured cross-relaxation rates and coupling constants, as observed herein.

3.6. Comparison between the conformation of HA_8 and HA_{20}

Thus far, there is no clear conclusion whether the conformation of HA oligosaccharides in aqueous solution can accurately represent the conformation of its longer chains. Previous studies combining NMR analysis and MD simulations have primarily focused on shorter oligosaccharides (Almond et al., 2006; Donati et al., 2001; Holmbeck et al., 1994; Sattelle et al., 2015). NMR studies on amide protons (Blundell, DeAngelis, & Almond, 2006; Cowman et al., 1984) and hydroxyl protons (Nestor & Sandström, 2017) of HA_8 and HA polymers found that their properties including chemical shifts and temperature coefficients are similar. Notably, these studies only focused on the interior part of HA_8 because terminal residues of oligosaccharides are typically more mobile than the interior residues (Cowman et al., 2001). Previous studies have observed chemical shift differences that indicate perturbed conformations and dynamics at the terminal residues of HA oligosaccharides (Blundell, Reed, & Almond, 2006). Therefore, end effects and local chain dynamics may influence the average values of proton distances in short oligosaccharide chains, and longer HA chains such as HA_{20} are less affected by these issues.

Our data suggest that there are only small differences in the conformation between HA_8 and HA_{20}. Both chain lengths showed almost identical conformations of the *N*-acetyl group and the glycosidic linkages, except for a 20° difference of ψ_{13} and a larger amount of *anti* conformation over the $\beta(1 \rightarrow 4)$ linkage in HA_{20}. However, it should be pointed out that HA_{20} is still much shorter than the native HA polymers and it is still an open question whether these effects are more pronounced when going to longer chain lengths or whether other effects are more important.

When comparing the overall structures of the 2BVK model and our NMR-derived models of HA_8 and of HA_{20}, the structures are similar resembling a four-fold left-handed helix (Fig. 6). The axial rise per disaccharide is predicted to be 8.8 Å in HA_8 and 7.4 Å in HA_{20}, which can be compared to the 2BVK model (8.4 Å) (Almond et al., 2006) and X-ray fiber diffraction refinement of sodium hyaluronate (8.5 Å; PDB accession code 2HYA) (Guss et al., 1975). However, the predicted *anti* conformation of $\beta(1 \rightarrow 4)$ linkages induces a twist similar to a hairpin (Fig. 6d), which creates a structure that is completely different from the elongated structure. Given that each HA_{20} is predicted to have an average of 1.5 $\beta(1 \rightarrow 4)$ linkages with an *anti* conformation (conformer II or II′), the twisted structure (Fig. 6d) is a more likely representation of HA_{20} than the elongated structure (Fig. 6c). Whether the hairpin-like structure is stabilized by inter-strand interactions (hydrogen bonding or ionic interactions), similarly to other glycan hairpins found recently (Fittolani et al., 2023; Yadav et al., 2024), remains to be investigated experimentally.

According to MD simulations, the formation of the hairpin-like structure is induced by interactions with a sodium ion (Kutálková et al., 2020). Since the present study was performed with the sodium salt of HA, such interactions are expected. Further studies could be done to investigate the role of the counterion, whether the type of ion and its concentration have an impact on the proportion of hairpin-like structures formed. Kutálková et al. (2020) concluded that there is a salt-dependent variation of the formation of temporary hairpin-like-structures and related this to a decrease of the end-to-end distance at higher salt concentration.

4. Conclusions

According to our NMR data and comparisons with model structures, there is no significant difference in the acetamide group between HA_8 and HA_{20}, and the torsion angle θ_1 of both chain lengths follows a clear *anti* conformation. As for the $\beta(1 \rightarrow 3)$ glycosidic linkage, the NMR data support the presence of a single predominant conformation for both chain lengths. The global minima of (φ_{13}, ψ_{13}) for HA_8 and HA_{20} are located at ((46 ± 6)°, (15 ± 9)°) and ((51 ± 7)°, (35 ± 18)°),

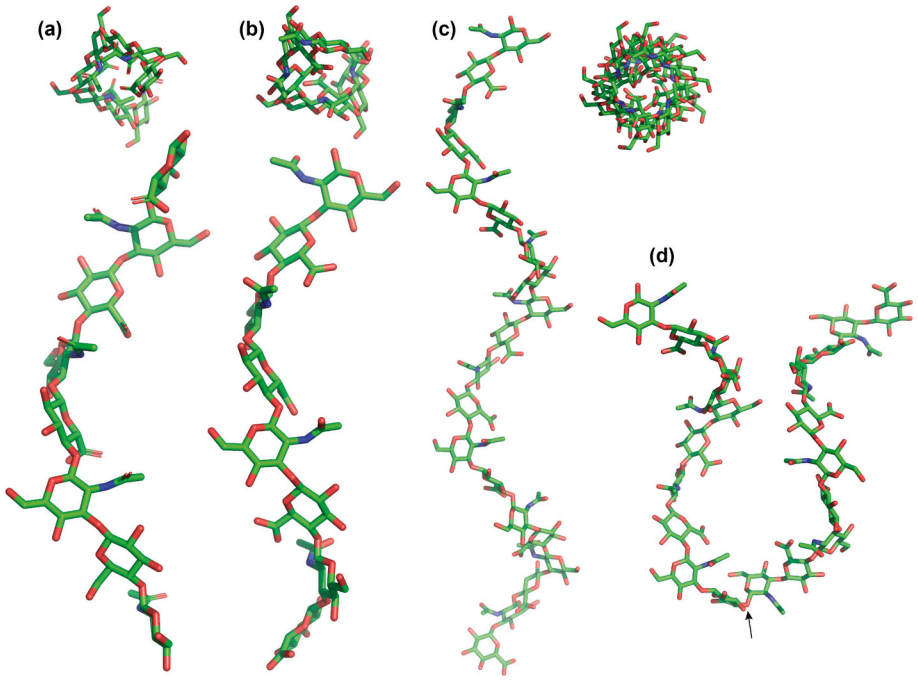

Fig. 6. (a) Average solution structure from MD simulations of HA_8 (2BVK, Almond et al. (2006)), (b) NMR-derived solution structure of HA_8, (c) NMR-derived solution structure of HA_{20}, and (d) NMR-derived solution structure of HA_{20} with conformer II between residue 10 and 11 (marked with an arrow). Note that structure a has a reducing-end GlcA whereas structure b-d have a reducing-end GlcNAc. Structure b-d were generated with CarbBuilder (Kuttel et al., 2016).

respectively. Finally, for the $\beta(1 \rightarrow 4)$ glycosidic linkage, NMR data did not match with one single conformation, indicating the presence of a conformational equilibrium at this linkage. By employing one *syn* and two *anti* conformations from previous MD simulations, the major *syn* conformation was predicted to be the same for both chain lengths. However, two minor *anti* conformations were equivalent to the NMR data of HA_{20}, accounting for 8 % and 9 %, respectively. In contrast, only one minor *anti* conformation was predicted from NMR data of HA_8, accounting for 8 % of the total. Overall, the conformations of HA_8 and HA_{20} at the glycosidic linkages exhibit subtle differences. This is the first NMR study that provides the substantiation for the existence of minor conformations over the $\beta(1 \rightarrow 4)$ glycosidic linkage, along with validation of the $\beta(1 \rightarrow 3)$ conformation previously established by MD simulations.

This study highlights the usefulness of NMR to provide experimental evidence that can be compared with predictions made by MD simulations. We anticipate that liquid-state NMR will be crucial for further investigations of HA in solution and solid-state NMR will be of great importance for conformational studies on high-molecular weight HA, as shown recently by the group of van der Wel (Rampratap et al., 2024).

CRediT authorship contribution statement

Yan Xue: Writing – review & editing, Writing – original draft, Visualization, Investigation, Formal analysis, Conceptualization. **Corine Sandström:** Writing – review & editing, Supervision, Resources, Project administration, Funding acquisition, Conceptualization. **Gustav Nestor:** Writing – review & editing, Visualization, Validation, Supervision, Software, Project administration, Methodology, Investigation, Formal analysis, Data curation, Conceptualization.

Declaration of competing interest

The authors declare that they have no known competing financial interests or personal relationships that could have appeared to influence the work reported in this paper.

Acknowledgments

We would like to thank Dr. Christina Nord and Dr. Lena Lundqvist for their support with the preparation of HPLC and ÄKTA systems.

Appendix A. Supplementary data

Supplementary data to this article can be found online at https://doi.org/10.1016/j.carbpol.2025.124612.

Data availability

Data will be made available on request.

References

Almond, A. (2007). Hyaluronan. *Cellular and Molecular Life Sciences, 64*(13), 1591–1596. https://doi.org/10.1007/s00018-007-7032-z

Almond, A., DeAngelis, P. L., & Blundell, C. D. (2006). Hyaluronan: The local solution conformation determined by NMR and computer modeling is close to a contracted left-handed 4-fold helix. *Journal of Molecular Biology, 358*(5), 1256–1269. https://doi.org/10.1016/j.jmb.2006.02.077

Bax, A., Sklenár, V., & Summers, M. F. (1986). Direct identification of relayed nuclear Overhauser effects. *Journal of Magnetic Resonance, 70*(2), 327–331. https://doi.org/10.1016/0022-2364(86)90018-1

Blundell, C. D., DeAngelis, P. L., & Almond, A. (2006). Hyaluronan: The absence of amide-carboxylate hydrogen bonds and the chain conformation in aqueous solution are incompatible with stable secondary and tertiary structure models. *The Biochemical Journal, 396*(3), 487–498. https://doi.org/10.1042/bj20060085

Blundell, C. D., Reed, M. A. C., & Almond, A. (2006). Complete assignment of hyaluronan oligosaccharides up to hexasaccharides. *Carbohydrate Research, 341*(17), 2803–2815. https://doi.org/10.1016/j.carres.2006.09.023

Chen, F. C., Kakizaki, I., Yamaguchi, M., Kojima, K., Takagaki, K., & Endo, M. (2009). Novel products in hyaluronan digested by bovine testicular hyaluronidase. *Glycoconjugate Journal, 26*(5), 559–566. https://doi.org/10.1007/s10719-008-9200-2

Cowman, M. K. (2017). Hyaluronan and Hyaluronan fragments. In D. C. Baker (Ed.), *74. Advances in carbohydrate chemistry and biochemistry* (pp. 1–59). https://doi.org/10.1016/bs.accb.2017.10.001

Cowman, M. K., Cozart, D., Nakanishi, K., & Balazs, E. A. (1984). ^{1}H NMR of glycosaminoglycans and hyaluronic acid oligosaccharides in aqueous solution: The amide proton environment. *Archives of Biochemistry and Biophysics, 230*(1), 203–212. https://doi.org/10.1016/0003-9861(84)90101-2

Cowman, M. K., Feder-Davis, J., & Hittner, D. M. (2001). C-13 NMR studies of hyaluronan. 2. Dependence of conformational dynamics on chain length and solvent. *Macromolecules, 34*(1), 110–115. https://doi.org/10.1021/ma001082e

Cowman, M. K., Hittner, D. M., & Feder-Davis, J. (1996). C-13-NMR studies of hyaluronan: Conformational sensitivity to varied environment [article]. *Macromolecules, 29*(8), 2894–2902. https://doi.org/10.1021/ma951701x

Cross, L. C., & Klyne, W. (1976). Rules for the nomenclature of organic chemistry. Section E: Stereochemistry. *Pure and Applied Chemistry, 45*(1), 11–30. https://doi.org/10.1351/pac197645010011

Donati, A., Magnani, A., Bonechi, C., Barbucci, R., & Rossi, C. (2001). Solution structure of hyaluronic acid oligomers by experimental and theoretical NMR, and molecular dynamics simulation. *Biopolymers, 59*(6), 434–445. https://doi.org/10.1002/1097-0282(200111)59:6<434::AID-BIP1048>3.0.CO;2-4

Fakhari, A., & Berkland, C. (2013). Applications and emerging trends of hyaluronic acid in tissue engineering, as a dermal filler and in osteoarthritis treatment. *Acta Biomaterialia, 9*(7), 7081–7092. https://doi.org/10.1016/j.actbio.2013.03.005

Fittolani, G., Tyrikos-Ergas, T., Poveda, A., Yu, Y., Yadav, N., Seeberger, P. H., … Delbianco, M. (2023). Synthesis of a glycan hairpin. *Nature Chemistry, 15*(10), 1461 +. https://doi.org/10.1038/s41557-023-01255-5

Florová, P., Sklenovsky, P., Banás, P., & Otyepka, M. (2010). Explicit water models affect the specific solvation and dynamics of unfolded peptides while the conformational behavior and flexibility of folded peptides remain intact. *Journal of Chemical Theory and Computation, 6*(11), 3569–3579. https://doi.org/10.1021/ct1003687

Fraser, J. R. E., Laurent, T. C., & Laurent, U. B. G. (1997). Hyaluronan: Its nature, distribution, functions and turnover. *Journal of Internal Medicine, 242*(1), 27–33. https://doi.org/10.1046/j.1365-2796.1997.00170.x

Gargiulo, V., Morando, M. A., Silipo, A., Nurisso, A., Pérez, S., Imberty, A., … De Castro, C. (2010). Insights on the conformational properties of hyaluronic acid by using NMR residual dipolar couplings and MD simulations. *Glycobiology, 20*(10), 1208–1216. https://doi.org/10.1093/glycob/cwq067

Giubertoni, G., Burla, F., Martinez-Torres, C., Dutta, B., Pletikapic, G., Pelan, E., … Bakker, H. J. (2019). Molecular origin of the elastic state of aqueous hyaluronic acid. *Journal of Physical Chemistry B, 123*(14), 3043–3049. https://doi.org/10.1021/acs.jpcb.9b00982

Giubertoni, G., Koenderink, G. H., & Bakker, H. J. (2019). Direct observation of intrachain hydrogen bonds in aqueous hyaluronan. *Journal of Physical Chemistry A, 123*(38), 8220–8225. https://doi.org/10.1021/acs.jpca.9b06462

Giubertoni, G., Ortíz, A. P. D., Bano, F., Zhang, X., Linhardt, R. J., Green, D. E., … Bakker, H. J. (2021). Strong reduction of the chain rigidity of hyaluronan by selective binding of Ca2+ ions. *Macromolecules, 54*(3), 1137–1146. https://doi.org/10.1021/acs.macromol.0c02242

Gold, E. W. (1982). Purification and properties of hyaluronidase from human-liver - differences from and similarities to the testicular enzyme. *Biochemical Journal, 205*(1), 69–74. https://doi.org/10.1042/bj2050069

Guss, J. M., Hukins, D. W. L., Smith, P. J. C., Winter, W. T., Arnott, S., Moorhouse, R., & Rees, D. A. (1975). Hyaluronic acid: Molecular conformations and interactions in two sodium salts. *Journal of Molecular Biology, 95*(3), 359–384. https://doi.org/10.1016/0022-2836(75)90196-5

Guvench, O. (2022). Atomic-resolution experimental structural biology and molecular dynamics simulations of hyaluronan and its complexes. *Molecules, 27*(21), Article 7276. https://doi.org/10.3390/molecules27217276

Hargittai, I., & Hargittai, M. (2008). Molecular structure of hyaluronan: An introduction. *Structural Chemistry, 19*(5), 697–717. https://doi.org/10.1007/s11224-008-9370-3

Heatley, F., & Scott, J. E. (1988). A water molecule participates in the secondary structure of hyaluronan. *The Biochemical Journal, 254*(2), 489–493. https://doi.org/10.1042/bj2540489

Holmbeck, S. M. A., Petillo, P. A., & Lerner, L. E. (1994). The solution conformation of hyaluronan: A combined NMR and molecular dynamics study. *Biochemistry, 33*(47), 14246–14255. https://doi.org/10.1021/bi00251a037

Hu, H. T., & Krishnamurthy, K. (2006). Revisiting the initial rate approximation in kinetic NOE measurements. *Journal of Magnetic Resonance, 182*(1), 173–177. https://doi.org/10.1016/j.jmr.2006.06.009

Hu, X. S., Carmichael, I., & Serianni, A. S. (2010). N-acetyl side-chains in saccharides: NMR J-coupling equations sensitive to CH-NH and NH-CO bond conformations in 2-acetamido-2-deoxy-aldohexopyranosyl rings. *Journal of Organic Chemistry, 75*(15), 4899–4910. https://doi.org/10.1021/jo100521g

Hu, X. S., Zhang, W. H., Carmichael, I., & Serianni, A. S. (2010). Amide cis-trans isomerization in aqueous solutions of methyl N-formyl-D-glucosaminides and methyl N-acetyl-D-glucosaminides: Chemical equilibria and exchange kinetics. *Journal of the American Chemical Society, 132*(13), 4641–4652. https://doi.org/10.1021/ja9086787

Kaufmann, J., Möhle, K., Hofmann, H. J., & Arnold, K. (1998). Molecular dynamics study of hyaluronic acid in water. *Journal of Molecular Structure-Theochem, 422*, 109–121. https://doi.org/10.1016/S0166-1280(97)00084-5

Klyne, W., & Prelog, V. (1960). Description of steric relationships across single bonds. *Experientia, 16*(12), 521–523. https://doi.org/10.1007/bf02158433

Kolmer, A., Edwards, L. J., Kuprov, I., & Thiele, C. M. (2015). Conformational analysis of small organic molecules using NOE and RDC data: A discussion of strychnine and α-methylene-γ-butyrolactone. *Journal of Magnetic Resonance, 261*, 101–109. https://doi.org/10.1016/j.jmr.2015.10.007

Kutálková, E., Hrncirík, J., Witasek, R., & Ingr, M. (2020). Effect of solvent and ions on the structure and dynamics of a hyaluronan molecule. *Carbohydrate Polymers, 234*, Article 115919. https://doi.org/10.1016/j.carbpol.2020.115919

Kuttel, M. M., Ståhle, J., & Widmalm, G. (2016). CarbBuilder: Software for building molecular models of complex oligo- and polysaccharide structures. *Journal of Computational Chemistry, 37*(22), 2098–2105. https://doi.org/10.1002/jcc.24428

Laurent, T. C. (1955). Studies on hyaluronic acid in the vitreous body. *Journal of Biological Chemistry, 216*(1), 263–271. https://doi.org/10.1016/S0021-9258(19)52303-1

Laurent, T. C., & Fraser, J. R. E. (1992). Hyaluronan. *FASEB Journal, 6*(7), 2397–2404. https://doi.org/10.1096/fasebj.6.7.1563592

Laurent, T. C., Ryan, M., & Pietruszkiewicz, A. (1960). Fractionation of hyaluronic acid - the polydispersity of hyaluronic acid from the bovine vitreous body. *Biochimica et Biophysica Acta, 42*(3), 476–485. https://doi.org/10.1016/0006-3002(60)90826-x

Lutsyk, V., & Plazinski, W. (2021). Conformational properties of glycosaminoglycan disaccharides: A molecular dynamics study. *Journal of Physical Chemistry B, 125*(39), 10900–10916. https://doi.org/10.1021/acs.jpcb.1c04860

Macura, S., Farmer, B. T., & Brown, L. R. (1986). An improved method for the determination of cross-relaxation rates from NOE data. *Journal of Magnetic Resonance, 70*(3), 493–499. https://doi.org/10.1016/0022-2364(86)90143-5

Meissner, A., & Sørensen, O. W. (2001). Measurement of J(H,H) and long-range J(X,H) coupling constants in small molecules. Broadband XLOC and J-HMBC. *Magnetic Resonance in Chemistry, 39*(1), 49–52. https://doi.org/10.1002/1097-458x(200101)39:1<49::Aid-mrc798>3.0.Co;2-s

Nestor, G., Kenne, L., & Sandström, C. (2010). Experimental evidence of chemical exchange over the β(1→3) glycosidic linkage and hydrogen bonding involving hydroxy protons in hyaluronan oligosaccharides by NMR spectroscopy [10.1039/B927159G]. *Organic & Biomolecular Chemistry, 8*(12), 2795–2802. https://doi.org/10.1039/b927159g

Nestor, G., & Sandström, C. (2017). NMR study of hydroxy and amide protons in hyaluronan polymers. *Carbohydrate Polymers, 157*, 920–928. https://doi.org/10.1016/j.carbpol.2016.10.005

Rampratap, P., Lasorsa, A., Arunachalam, A., Kamperman, M., Walvoort, M. T. C., & van der Wel, P. C. A. (2024). Resolving atomic-level dynamics and interactions of high-molecular-weight hyaluronic acid by multidimensional solid-state NMR. *ACS Applied Materials & Interfaces, 16*(33), 43317–43328. https://doi.org/10.1021/acsami.4c08428

Sattelle, B. M., Shakeri, J., Cliff, M. J., & Almond, A. (2015). Proteoglycans and their heterogeneous glycosaminoglycans at the atomic scale. *Biomacromolecules, 16*(3), 951–961. https://doi.org/10.1021/bm5018386

Säwén, E., Massad, T., Landersjö, C., Damberg, P., & Widmalm, G. (2010). Population distribution of flexible molecules from maximum entropy analysis using different priors as background information: Application to the ϕ, ψ-conformational space of the α-(1→2)-linked mannose disaccharide present in N- and O-linked glycoproteins. *Organic & Biomolecular Chemistry, 8*(16), 3684–3695. https://doi.org/10.1039/c003958f

Scott, J. E., & Heatley, F. (1999). Hyaluronan forms specific stable tertiary structures in aqueous solution: A ^{13}C NMR study. *Proceedings of the National Academy of Sciences of the United States of America, 96*(9), 4850–4855. https://doi.org/10.1073/pnas.96.9.4850

Sheehan, J. K., & Atkins, E. D. T. (1983). X-ray fiber diffraction study of conformational-changes in hyaluronate induced in the presence of sodium, potassium and calcium cations. *International Journal of Biological Macromolecules, 5*(4), 215–221. https://doi.org/10.1016/0141-8130(83)90005-3

Taweechat, P., Pandey, R. B., & Sompornpisut, P. (2020). Conformation, flexibility and hydration of hyaluronic acid by molecular dynamics simulations. *Carbohydrate Research, 493*, Article 108026. https://doi.org/10.1016/j.carres.2020.108026

van Dam, E. P., Giubertoni, G., Burla, F., Koenderink, G. H., & Bakker, H. J. (2020). Hyaluronan biopolymers release water upon pH-induced gelation. *Physical Chemistry Chemical Physics, 22*(16), 8667–8671. https://doi.org/10.1039/d0cp00215a

Volpi, N. (2007). On-line HPLC/ESI-MS separation and characterization of hyaluronan oligosaccharides from 2-mers to 40-mers. *Analytical Chemistry, 79*(16), 6390–6397. https://doi.org/10.1021/ac070837d

Weissmann, B., Meyer, K., Sampson, P., & Linker, A. (1954). Isolation of oligosaccharides enzymatically produced from hyaluronic acid. *Journal of Biological Chemistry, 208*(1), 417–429. https://doi.org/10.1016/S0021-9258(18)65660-1

Whitmore, E. K., Martin, D., & Guvench, O. (2020). Constructing 3-dimensional atomic-resolution models of nonsulfated glycosaminoglycans with arbitrary lengths using conformations from molecular dynamics. *International Journal of Molecular Sciences, 21*(20), Article 7699. https://doi.org/10.3390/ijms21207699

Willker, W., & Leibfritz, D. (1995). Determination of heteronuclear long-range H,X coupling-constants from gradient-selected HMBC spectra. *Magnetic Resonance in Chemistry, 33*(8), 632–638. https://doi.org/10.1002/mrc.1260330804

Xue, Y., & Nestor, G. (2022). Determination of amide cis/trans isomers in N-acetyl-d-glucosamine: Tailored NMR analysis of the N-acetyl group conformation. *Chembiochem, 23*(17), Article e202200338. https://doi.org/10.1002/cbic.202200338

Yadav, N., Djalali, S., Poveda, A., Ricardo, M. G., Seeberger, P. H., Jiménez-Barbero, J., & Delbianco, M. (2024). Dissecting the conformational stability of a glycan hairpin. *Journal of the American Chemical Society, 146*(9), 6369–6376. https://doi.org/10.1021/jacs.4c00423